

Cite this article as: Zhang Yunsheng, Jiang Xueyu, Zhou Ge, et al. Comparison of Different Instability Criteria for Processing Maps of NiCoFeCrAl High Entropy Alloy[J]. Rare Metal Materials and Engineering, 2024, 53(01): 38-46. DOI: 10.12442/j.issn.1002-185X.E20230037.

ARTICLE

Comparison of Different Instability Criteria for Processing Maps of NiCoFeCrAl High Entropy Alloy

Zhang Yunsheng^{1,2}, Jiang Xueyu^{1,2}, Zhou Ge^{1,2}, Zhang Haoyu^{1,2}, Zhang Siqian^{1,2},
Che Xin^{1,2}, Chen Lijia^{1,2}, Cao Xue³

¹ School of Materials Science and Engineering, Shenyang University of Technology, Shenyang 110870, China; ² Shenyang Key Laboratory of Advanced Structural Materials and Applications, Shenyang University of Technology, Shenyang 110870, China; ³ AECC Beijing Institute of Aeronautical Materials, Beijing 100095, China

Abstract: The single-pass thermal compression experiments were conducted on NiCoFeCrAl high entropy alloy by Gleeble-3800 thermal simulation tester. The Arrhenius constitutive model was established based on the peak stresses. With four instability criteria (Prasad, Murty, Gegel, and Malas), different heat processing maps of dynamic material model were established. The applicable ranges of the instability criteria for the alloys in the heat deformation process were analyzed and compared. Results show that the optimal heat processing ranges of the alloys are the temperature range of 980–1010 °C+strain rate of 0.01–0.001 s⁻¹ and the temperature range of 1050–1100 °C+strain rate of 0.01–0.1 s⁻¹. The average power dissipation rate is greater than 36%. Through EBSD microstructure analysis, the softening mechanism of thermal deformation is changed from dynamic recovery to dynamic recrystallization with increasing the deformation amount.

Key words: high entropy alloy; instability criterion; thermal deformation behavior; Arrhenius constitutive equation; distortion organization

High entropy alloys are different from the traditional alloys: they are composed of five or more equal or nearly equal metals, and the concentration of each constituent element is 8at% – 35at%. The design of equal atomic ratio of metal elements in the multi-major-element alloys^[1-3] reflects the chaotic principle, which is also the basis for the establishment of new alloys. When the mixing entropy $\Delta S_{\text{mix}} > 1.61R$, high entropy alloys can be obtained^[4]. Because high entropy alloys usually possess high entropy effect^[5], lattice distortion effect^[6], slow diffusion effect^[7], and cocktail effect^[8], they have better organization and mechanical properties than the traditional alloys do. Compared with the traditional alloys, high entropy alloys have the characteristics of high strength, high hardness^[9], good corrosion resistance^[10-11], and superior thermal stability^[12]. The element diffusion inside high entropy alloys requires the synergistic diffusion of various elements, which is difficult for the growth of new phases. Nanometer-sized precipitate phases often appear in high entropy alloys,

thereby further improving the strength and hardness of alloys. Heat deformation is one of the indispensable traditional treatments for metal processing, and the influence of heat deformation process parameters on organization evaluation and mechanical properties is significant. The hot deformation process parameters, such as strain rate and deformation temperature, are essential to control the microstructure of the final products^[13]. Abnormal deformation conditions usually lead to surface cracks, uneven grain size distribution, and rheological inhomogeneity^[14-15]. Work hardening, dynamic softening, and other more complex evolution processes usually occur in the hot deformation process^[16].

Appropriate hot deformation process can eliminate cast-state tissue defects, improve organization, and enhance mechanical properties. Therefore, the thermal processing map is often used to design and ameliorate the metal thermal processing process. Unstable rheological regions should be avoided during thermal processing, and the reference stable

Received date: September 18, 2023

Foundation item: Natural Science Foundation Special (22-315-6-04)

Corresponding author: Zhou Ge, Ph. D., School of Materials Science and Engineering, Shenyang University of Technology, Shenyang 110870, P. R. China, E-mail: zhouge@sut.edu.cn

Copyright © 2024, Northwest Institute for Nonferrous Metal Research. Published by Science Press. All rights reserved.

reological regions can be clearly observed in the thermal processing map. The instability criteria based on the dynamic material model (DMM) mainly include the Prasad instability criterion, Gegel instability criterion, Malas instability criterion, and Murty instability criterion. At present, the Prasad instability criterion is the most widely used one, which can accurately depict the thermal processing map of Ti alloys^[17] and Mg alloys^[18]. Besides, the desirable processing intervals and instability intervals can be obtained from the thermal processing map. The thermal forming production within the instability interval can lead to lousy processing feasibility, and cracks as well as other defects will be generated inside the alloys^[19]. However, the instability conditions of other instability criteria are rarely investigated, and the thermal deformation behavior of NiCoFeCrAl high entropy alloys should be further clarified.

In this research, four instability criteria of NiCoFeCrAl high entropy alloy were established, and the applicable ranges of different instability criteria were analyzed and compared. Single-pass thermal compression experiments were conducted by the Gleeble-3800 thermal simulation tester for the self-designed nickel-based lightweight high entropy alloys. The Arrhenius constitutive model under peak stress was established based on the stress-strain curves under different deformation processes in order to study the thermal deformation behavior of NiCoFeCrAl high entropy alloy. The thermal processing diagrams under the Prasad, Murty, Gegel, and Malas instability criteria were plotted to determine the thermal processing characteristics of alloys under different conditions. Electron backscattered diffraction (EBSD) analysis was used to investigate the microstructure evolution mechanism of NiCoFeCrAl high entropy alloy during thermal deformation process. This research provided essential theoretical basis for the design and optimization of process parameters for the actual production and processing of NiCoFeCrAl high entropy alloy.

1 Experiment

The raw material was nickel-based high entropy alloy, Ni-8.0Al-20.0Co-10.0Cr-18.5Fe-7.0Mo-1.0Nb-2.0Ti-3.0W-0.04C (wt%), and it was called as NiCoFeCrAl high entropy alloy in this research. The specimens were machined into the cylindrical ones with dimension of $\Phi 10 \text{ mm} \times 15 \text{ mm}$ by wire-cutting, and the surface oxide skin was ground by sandpaper. The hot compression tests were conducted by Gleeble-3800 thermal simulating tester. The temperature was from 900 °C to 1100 °C with temperature interval of 50 °C, and the strain rate was from 0.001 s⁻¹ to 1 s⁻¹. The height reduction ratio was 0.6. After reaching the deformation temperature at heating rate of 10 °C/s, the specimen was kept for 3 min to achieve a uniform temperature distribution. After the compression test was completed, the specimen was immediately subjected to water-cooling and then placed at room temperature to preserve the microstructure during high-temperature deformation.

The deformed specimen was cut along the compression axial direction to observe the microstructure. Due to the

inhomogeneity of the thermal compression deformation process, the microstructure observation was mainly conducted in the central part of the specimen. Before EBSD observation, the specimen was mechanically and electrolytically polished in 10vol% perchloric acid+90vol% ethanol solution under the voltage of 25 V and current of 0.9–1.1 A. EBSD analysis was conducted by Channel 5 software.

2 Results and Discussion

2.1 Peak flow stress

During the thermal compression experiments, the peak stresses under different process parameters were recorded, and the peak stress is changed with changing the deformation temperature and the strain rate. As shown in Fig. 1, under the same strain rate, the peak stress is decreased with increasing the deformation temperature. Under the same temperature, with decreasing the deformation rate, the peak stress is decreased. It can be seen that the hot compression deformation behavior of NiCoFeCrAl high entropy alloy has typical strain rate sensitivity characteristics. The deformation resistance at low temperatures and high strain rates is much higher than that at high temperatures and low strain rates. Higher deformation resistance indicates the higher resistance against the hot working process. This result suggests that the instability probably occurs under the thermal processing conditions of low temperature and high strain rate.

2.2 Constitutive model

The Arrhenius hyperbolic sine functional equation^[20] is commonly used to represent the intrinsic relationship of NiCoFeCrAl high entropy alloy during thermal deformation process:

$$\dot{\epsilon} = A_1 \sigma^n \exp\left(-\frac{Q}{RT}\right) \quad \alpha\sigma < 0.8 \quad (1)$$

$$\dot{\epsilon} = A_2 \exp(\beta\sigma) \exp\left(-\frac{Q}{RT}\right) \quad \alpha\sigma > 1.2 \quad (2)$$

$$\dot{\epsilon} = A [\sinh(\alpha\sigma)]^n \exp\left(-\frac{Q}{RT}\right) \quad \text{For all } \alpha\sigma \quad (3)$$

where $\dot{\epsilon}$ is the strain rate; σ is the stress (MPa); R is the gas constant (kJ·mol⁻¹·K⁻¹); Q is the activation energy of thermal deformation (kJ/mol); A_1 , A_2 , A , n_1 , n , α , and β are the material

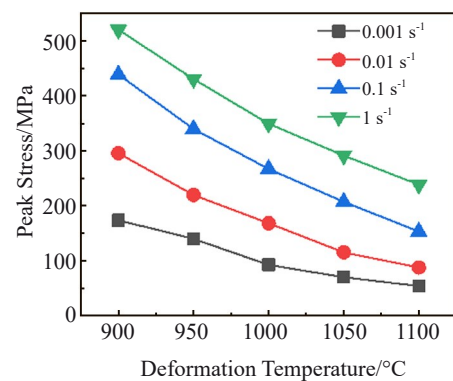


Fig.1 Peak stress at different deformation temperatures and strain rates

constants and $\alpha=\beta/n_1$.

By taking the natural logarithm on both sides of Eq.(1–3), Eq.(4–6) can be obtained, respectively:

$$\ln \dot{\epsilon} = \ln A_1 + n_1 \ln \sigma - Q/RT \quad (4)$$

$$\ln \dot{\epsilon} = \ln A_2 + \beta \sigma - Q/RT \quad (5)$$

$$\ln \dot{\epsilon} = \ln A + n \ln [\sinh(\alpha \sigma)] - Q/RT \quad (6)$$

By taking the peak stress σ into Eq. (4) and Eq. (5), the relationship between strain rate and stress can be obtained, as shown in Fig. 2. n_1 and β can be obtained from the average slope, and then α can also be obtained. In this case, $n_1=5.23$, $\beta=0.026888$, and $\alpha=\beta/n_1=0.0051$.

According to Eq. (6), the plots of $\ln \dot{\epsilon} - \ln[\sinh(\alpha \sigma)]$ can be obtained, as shown in Fig. 3a. The average slope is 3.79181, and the deformation activation energy Q can be calculated. Eq. (7) can be obtained through the partial differentiation of both sides of Eq.(6), as follows:

$$Q = R \left| \frac{\partial \ln \dot{\epsilon}}{\partial \ln [\sinh(\alpha \sigma)]} \right|_T \cdot \left| \frac{\partial \ln [1/T]}{\partial \ln (1/T)} \right| \quad (7)$$

Then, the plots of $\ln[\sinh(\alpha \sigma)] - (1/T)$ are obtained, as shown in Fig. 3b. The average slope of $\ln[\sinh(\alpha \sigma)] - (1/T)$ plot is 7.48.

In addition, the Zener-Holloman parameter (Z) can represent the influence of temperature and strain rate on the thermal deformation behavior of materials^[21], and its expression is as follows:

$$Z = \dot{\epsilon} \exp(Q/RT) = A [\sinh(\alpha \sigma)]^n \quad (8)$$

The physical meaning of Z parameter is the temperature compensated strain rate factor. By taking the natural logarithm on both sides of Eq.(8), Eq.(9) is obtained, as follows:

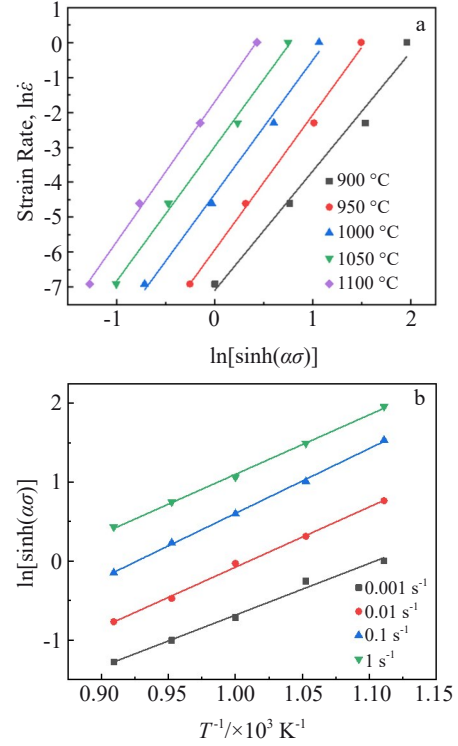


Fig.3 Relationships of $\ln \dot{\epsilon} - \ln[\sinh(\alpha \sigma)]$ (a) and $\ln[\sinh(\alpha \sigma)] - (1/T)$ (b)

$$\ln Z = n \ln [\sinh(\alpha \sigma)] + \ln A \quad (9)$$

Thus, the relationship of $\ln Z - \ln[\sinh(\alpha \sigma)]$ is obtained, as shown in Fig. 4. The material constant $n=3.77515$ and $A = e^{23.97179}$.

Therefore, the Arrhenius constitutive relationship model of NiCoFeCrAl high entropy alloy is as follows:

$$\sigma = 194.62826 \ln \left\{ \left(\frac{Z}{e^{23.97179}} \right)^{\frac{1}{3.77515}} + \left[\left(\frac{Z}{e^{23.97179}} \right)^{\frac{2}{3.77515}} + 1 \right]^{\frac{1}{2}} \right\} \quad (10)$$

$$\text{with } Z = e^{23.97179} [\sinh(0.005138\sigma)]^{3.77515}$$

The error analysis of this constitutive equation is conducted. The calculated and experimental peak rheological stresses are compared, as shown in Fig. 5. The complex correlation coefficient $R^2=0.99285$, which is very close to 1, indicating that the correlation between the two random

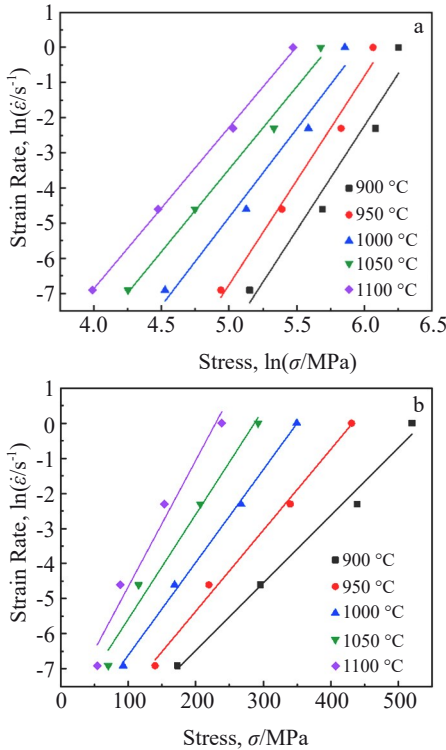


Fig.2 Relationships between strain rate and stress: (a) $\ln \dot{\epsilon} - \ln \sigma$ and (b) $\ln \dot{\epsilon} - \sigma$

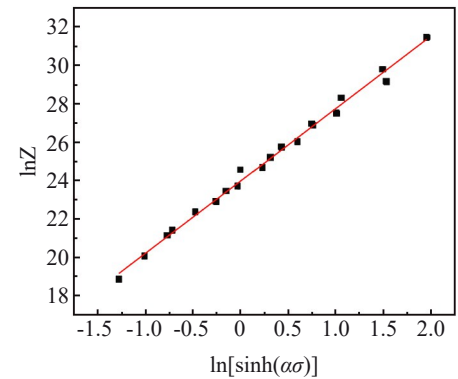


Fig.4 Relationship between $\ln Z$ and $\ln[\sinh(\alpha \sigma)]$

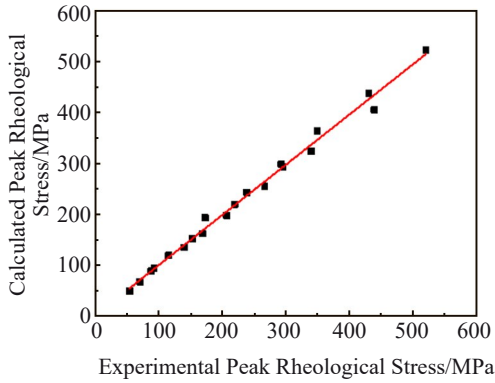


Fig.5 Error analysis of calculated and experimental peak rheological stresses

variables is very strong and this constitutive relationship can accurately predict the rheological stress of NiCoFeCrAl alloy during heat deformation.

2.3 Hot working maps under different instability criteria

The energy P can be divided into two parts: the dissipative quantity (G) and the dissipative covariate (J), as follows:

$$P = \sigma \dot{\epsilon} = G + J = \int_0^{\dot{\epsilon}} \sigma d\dot{\epsilon} + \int_0^{\sigma} \dot{\epsilon} d\sigma \quad (11)$$

where G is the energy consumed by the material during plastic deformation; J is the energy dissipated by the evolution of microstructure during material deformation. The proportion of these two energy types is determined by the strain rate sensitivity index m of the workpiece under certain stress, as follows:

$$m = \frac{\partial J}{\partial G} = \dot{\epsilon} \frac{\partial \sigma}{\partial \dot{\epsilon}} = \frac{\partial \ln \sigma}{\partial \ln \dot{\epsilon}} \quad (12)$$

The dissipation of material energy can be divided into two parts: potential energy and kinetic energy. Changes in microstructure will inevitably cause changes in the atomic potential energy, thus influencing the dissipation covariate J . The movement of dislocations and the transformation of kinetic energy are influenced by the form of thermal energy. Thus, the integral of the dissipation covariate J corresponding to the dissipation amount G can be expressed, as follows:

$$dJ = \dot{\epsilon} d\sigma \quad (13)$$

Supposing that the material conforms to the constitutive relationship $\sigma = C\dot{\epsilon}$, J can be expressed as:

$$J = \int_0^{\dot{\epsilon}} \sigma d\dot{\epsilon} \quad (14)$$

When $m=1$, the material is at the ideal linear dissipative state, and the dissipative covariance J reaches the maximum value J_{\max} , as follows:

$$J_{\max} = \frac{\sigma \dot{\epsilon}}{2} \quad (15)$$

A dimensionless parameter η can be obtained from Eq.(14) and Eq. (15), which reflects the power dissipation rate, as follows:

$$\eta = \frac{J}{J_{\max}} = 2m/(m+1) \quad (16)$$

Four instability criteria (Prasad, Gegel, Malas, and Murthy)

are used in this research. Doraivelu et al^[22] studied the relationship between the rheological instability during material deformation and the temperature-sensitive parameter S based on the second law of thermodynamics. The parameter S can be expressed, as follows:

$$S = \frac{1}{T} \frac{\partial \ln \sigma}{\partial \frac{1}{T}} = \frac{\partial \ln \sigma}{\partial \ln T} \quad (17)$$

According to the Gegel criterion, when the material reaches the steady-state stress, the overall rheological stress curve tends to present convex characteristic, and the power dissipation efficiency factor η is decreased with increasing the strain rate. Eq.(18) can be obtained, as follows:

$$\frac{\partial S}{\partial \ln \dot{\epsilon}} = -\frac{\partial (\partial \ln \sigma)}{\partial (\ln T) \partial (\ln \dot{\epsilon})} = -\frac{\partial m}{\partial (\ln T)} > 0 \Rightarrow \frac{\partial m}{\partial (\ln T)} < 0 \quad (18)$$

The Gegel instability criterion is based on the second law of thermodynamics, as follows:

$$\frac{\partial \eta}{\partial \ln \dot{\epsilon}} > 0 \quad \frac{\partial m}{\partial \ln T} < 0 \quad (19)$$

Malas et al^[23] introduced the Lyapunov function $L(\eta, \sigma)$, and the power dissipation efficiency factor η can be replaced by m . The Malas instability criterion is based on the Gegel criterion, as follows:

$$\frac{\partial m}{\partial \ln \dot{\epsilon}} > 0 \quad \frac{\partial m}{\partial \ln T} < 0 \quad (20)$$

Prasad et al^[24] proposed the theory of maximum entropy generation based on the results in Ref.[25]. The relationship between the dissipation function $D(\dot{\epsilon})$ and the strain rate satisfies the specific equation, as follows:

$$\frac{dD}{d\dot{\epsilon}} < \frac{D}{\dot{\epsilon}} \quad (21)$$

During the thermal deformation, since the dissipation coefficients are closely related to the organization evolution, the dissipation function in the abovementioned equation can be replaced by the dissipation coefficients^[26-27], as follows:

$$\frac{\partial J}{\partial \dot{\epsilon}} < \frac{J}{\dot{\epsilon}} \quad (22)$$

$$\frac{\partial (\ln J)}{\partial (\ln \dot{\epsilon})} < 1 \quad (23)$$

By taking natural logarithm on both sides of Eq.(14) and taking partial derivative of $\ln \dot{\epsilon}$, Eq.(24) can be obtained, as follows:

$$\frac{\partial \ln J}{\partial \ln \dot{\epsilon}} = \frac{\partial \ln \left(\frac{m}{m+1} \right)}{\partial \ln \dot{\epsilon}} + \frac{\partial \ln \sigma}{\partial \ln \dot{\epsilon}} + 1 \quad (24)$$

Prasad et al^[24] introduced the instability coefficient $\xi(\dot{\epsilon})$ into the instability criterion and proposed the Prasad instability criterion for the alloys during high-temperature deformation, as follows:

$$\xi(\dot{\epsilon}) = \frac{\partial \ln [m/(m+1)]}{\partial \ln \dot{\epsilon}} + m < 0 \quad (25)$$

Murthy^[28] and Spigarelli^[29] et al found that for the pure metals and alloys with low degree of alloying, m can be simply considered as a constant value. However, for the complex alloying situation, m cannot be considered as a constant, based on the Murthy criterion. Thus, the criterion of

unstable region for the stress-strain rate curves can be expressed, as follows:

$$J = \int_0^{\sigma} \dot{\epsilon} d\sigma \Rightarrow \frac{\partial J}{\partial \dot{\epsilon}} = \frac{\partial \sigma}{\partial \dot{\epsilon}} \dot{\epsilon} = \sigma \frac{\partial \ln \sigma}{\partial \ln \dot{\epsilon}} = m\sigma \quad (26)$$

$$\eta = \frac{J}{J_{\max}} = \frac{J}{\sigma \dot{\epsilon} / 2} \Rightarrow \frac{J}{\dot{\epsilon}} = \frac{1}{2} \eta \sigma \quad (27)$$

According to Eq. (22), the Murthy instability criterion can be obtained, as follows:

$$2m < \eta \quad (28)$$

The thermal processing maps of NiCoFeCrAl high entropy alloy based on four instability criteria under peak stress conditions are shown in Fig. 6. The shaded areas in Fig. 6 denote the processing instability intervals. It is worth mentioning that the DMM thermal processing map based on Murthy instability criterion has no instability interval. Based on the Prasad instability criterion, a large rheological instability region occurs in the temperature range of 900–1100 °C and strain rate of 0.082–1 s⁻¹, which indicates that this high-entropy high-temperature alloy is unsuitable for thermal processing under high strain rate conditions. The Malas instability criterion replaces η in the Gegel instability criterion with m . Therefore, the two criteria are similar, and the thermal processing maps based on these two criteria only show slight difference. There are two rheological instability regions based on the Malas and Gegel instability criteria: temperature range of 905–975 °C with strain rate of 0.01–0.001 s⁻¹ and the temperature range of 1020–1100 °C with strain rate of 0.01–0.001 s⁻¹. According to the prediction obtained by Prasad instability criterion, the instability region is concentrated in the region of high strain rate, and the power dissipation value

is low under this condition. The power dissipation value is less than 0.2. In the actual production and processing, the high η zone and the safe zone for processing should be selected as much as possible. The high η zone is usually considered as a suitable processing region, because the high η zone is more prone to dynamic recrystallization (DRX)^[30], which is beneficial to the heat deformation process. DRX softens the material, reduces the deformation resistance during deformation, refines microstructures, and improves the microstructure homogeneity, thus providing good machinability and flow stability. However, in the high η region, the production of a large number of defects may occur, which can also lead to the high power dissipation. Thus, the instability regions predicted by the Prasad, Gegel, and Malas instability criteria inevitably contain partial high power dissipation region.

The instability intervals based on the Prasad instability criterion are concentrated in the high strain rate region, and those based on the Gegel and Malas instability criteria are concentrated in the low-to-medium strain rate region. In order to verify the accuracy of the predicted results of different instability criteria, the cracking maps of heat-deformed specimens under different process parameters are analyzed, as shown in Fig. 7. Compared with the predicted results from the thermal processing maps in Fig. 6, the deformation parameters in the instability regions predicted by the Prasad instability criterion are 900 °C-1 s⁻¹, 950 °C-1 s⁻¹, 1000 °C-1 s⁻¹, 1050 °C-1 s⁻¹, and 1100 °C-1 s⁻¹. It can be seen that the hot compression specimens under different conditions show different degrees of cracking and deformation inhomogeneity, suggesting that the predicted results based on the Prasad

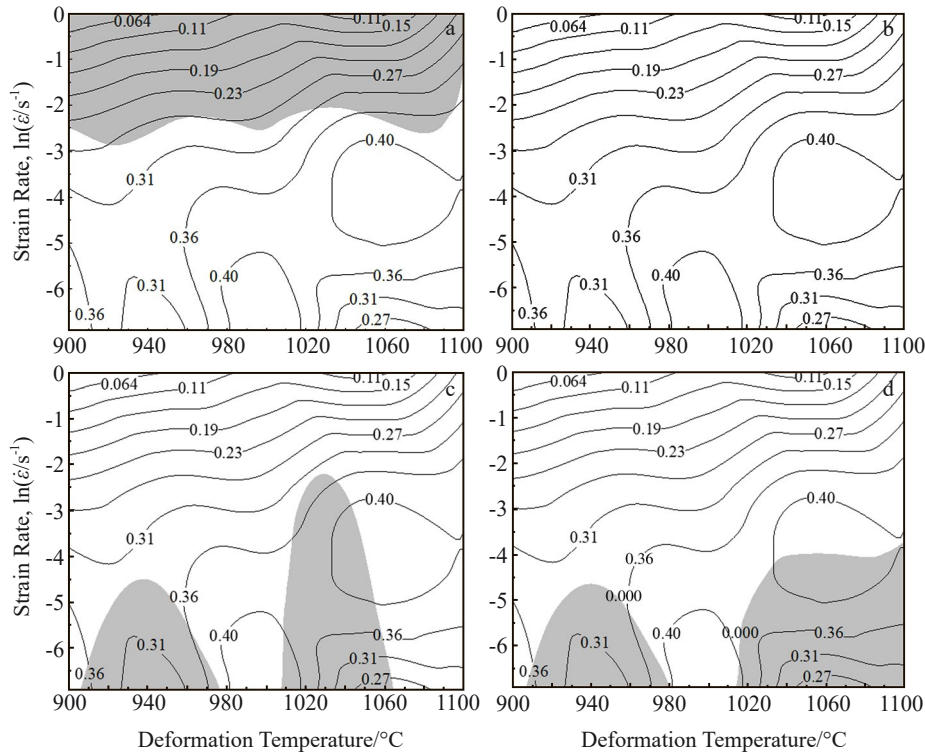


Fig.6 Thermal processing maps of NiCoFeCrAl high entropy alloy based on Prasad (a), Murthy (b), Gegel (c), and Malas (d) instability criteria

instability criterion are more accurate under these conditions. The corresponding deformation parameters in the instability region predicted by the Gegel and Malas instability criteria are $950\text{ }^{\circ}\text{C}-0.001\text{ s}^{-1}$, $1050\text{ }^{\circ}\text{C}-0.001\text{ s}^{-1}$, and $1100\text{ }^{\circ}\text{C}-0.001\text{ s}^{-1}$. It is clear that the hot compression specimens under these conditions all show cracking phenomena and polygonal inhomogeneous bulging characteristics, which indicates that the prediction results based on the Gegel and Malas instability criteria are more accurate. The analysis of the prediction results of the four instability criteria for NiCoFeCrAl high entropy alloy shows that the DMM heat processing map drawn by Murty instability criterion does not have instability intervals, which does not apply to the prediction of instability intervals of this alloy, and the prediction results of Prasad, Gegel, and Malas instability criteria are more accurate under these conditions. The prediction results of sole instability criterion for NiCoFeCrAl high entropy alloy is limited, and the combination of the prediction results of multiple instability criteria can predict the rheological instability region of the alloys more accurately during the heat deformation process.

2.4 Microstructure

According to Fig.6 and Fig.7, it can be seen that the specimens are deformed uniformly under the conditions of $1000\text{ }^{\circ}\text{C}/0.01-0.001\text{ s}^{-1}$ and $1050-1100\text{ }^{\circ}\text{C}/0.1\text{ s}^{-1}$. After compression, the specimens are uniformly bulged and have no cracks. No instability region can be observed. The power dissipation ratio is high, which indicates that the NiCoFeCrAl high entropy alloy has good thermoforming properties under the specific deformation conditions. Fig. 8a – 8d show EBSD maps of NiCoFeCrAl high entropy alloy after hot compression at temperature of $1000\text{ }^{\circ}\text{C}$ and strain rate of $1-0.001\text{ s}^{-1}$. The blue area represents the recrystallized (DRXed) grains, the

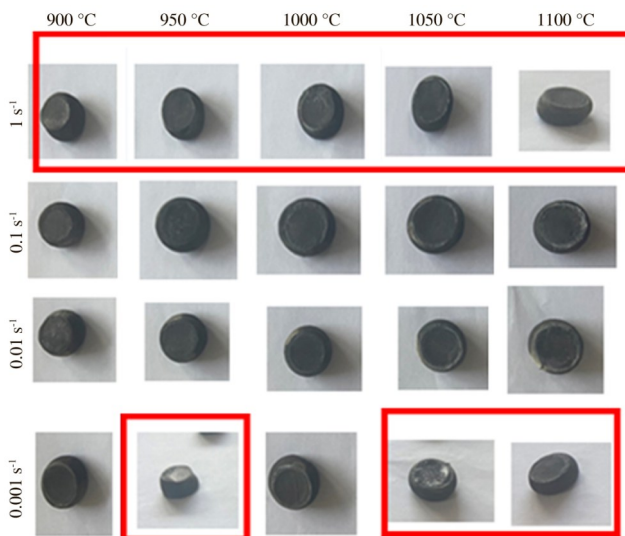


Fig.7 Cracking maps of NiCoFeCrAl high entropy alloy after hot compression under different deformation temperatures and strain rates (red rectangles denote the precise prediction results)

yellow area represents the sub-crystalline structural (substructured) organization, and the red area represents the deformed grains. It can be seen that the NiCoFeCrAl alloy is composed of a large number of primitive deformed grains, some sub-crystalline structures, and a small number of dynamically recrystallized grains when the strain rate is 1 s^{-1} . The sub-crystalline is the main product of dynamic recovery, indicating that the thermal compression process is accompanied by the occurrence of dynamic recovery to a large extent. The dynamic recovery is a continuous process. During the thermal compression, the internal dislocations in the grains continue to propagate, the density continues to increase, and a large number of dislocations are entangled. The cellular sub-structures are also formed during the thermal deformation process, which consumes a large number of dislocations, therefore exerting a significant softening effect. With decreasing the strain rate, DRX degree is increased, the proportion of original deformed grains is gradually decreased which are replaced by dynamically recrystallized grains and sub-crystalline structures, and the dynamically recrystallized grains tend to form distortion-free equiaxed grains. The main softening mechanism is changed from dynamic recovery to DRX, and the softening effect is further enhanced. The resultant phenomenon is that the peak stress of thermal compression is decreased with decreasing the strain rate (Fig.1). Under certain temperature conditions, when the strain rate is large, the thermal compression processing is fast, the dislocation climb/slip cannot sufficiently proceed, and the heterogeneous dislocations cannot be offset by mutual movement. Therefore, the dislocations are entangled with each other, and the energy storage is increased, which are all attributed to the high strain rate and short deformation duration, although the atoms cannot diffuse sufficiently at higher temperatures. Therefore, at high temperatures and high strain rates, DRX does not occur or DRX just begins. Thus, the recrystallized grains cannot grow sufficiently. With decreasing the strain rate, the dislocation climb/slip can proceed sufficiently, the dislocations of dissimilar signatures are mutually offset, and the stored energy is decreased. The alloys have sufficient time for recrystallization and growth of recrystallized grains when the strain rate is low. Thus, the optimal hot forming conditions are the temperature of $980-1010\text{ }^{\circ}\text{C}$ and strain rate of $0.01-0.001\text{ s}^{-1}$. In this case, DRX degree is high. The occurrence of DRX is beneficial to the thermal deformation behavior, which can refine the grains, eliminate the defects^[31], and reduce the deformation resistance during thermal deformation.

Fig. 9 shows EBSD maps and analysis results of NiCoFeCrAl high entropy alloy after hot compression at strain rate of 0.1 s^{-1} and temperature of $900-1100\text{ }^{\circ}\text{C}$. At the strain rate of 0.1 s^{-1} , with increasing the temperature, the deformed grains are gradually replaced by the dynamically recrystallized grains and sub-crystalline structures, the proportion of dynamically recrystallized grains is gradually increased, the proportion of the original deformed grains is gradually decreased, and the original grains are gradually

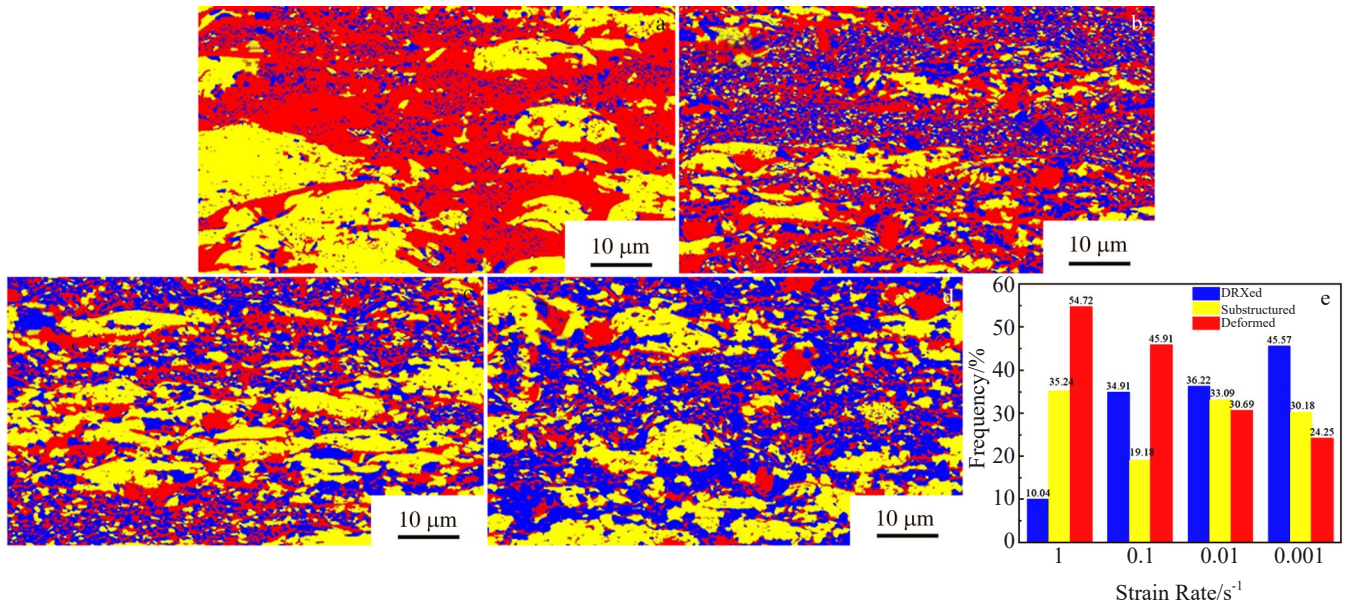


Fig.8 EBSD maps (a–d) and analysis results (e) of NiCoFeCrAl high entropy alloy after hot compression at temperature of 1000 °C and strain rate of 1 s⁻¹ (a), 0.1 s⁻¹ (b), 0.01 s⁻¹ (c), and 0.001 s⁻¹ (d)

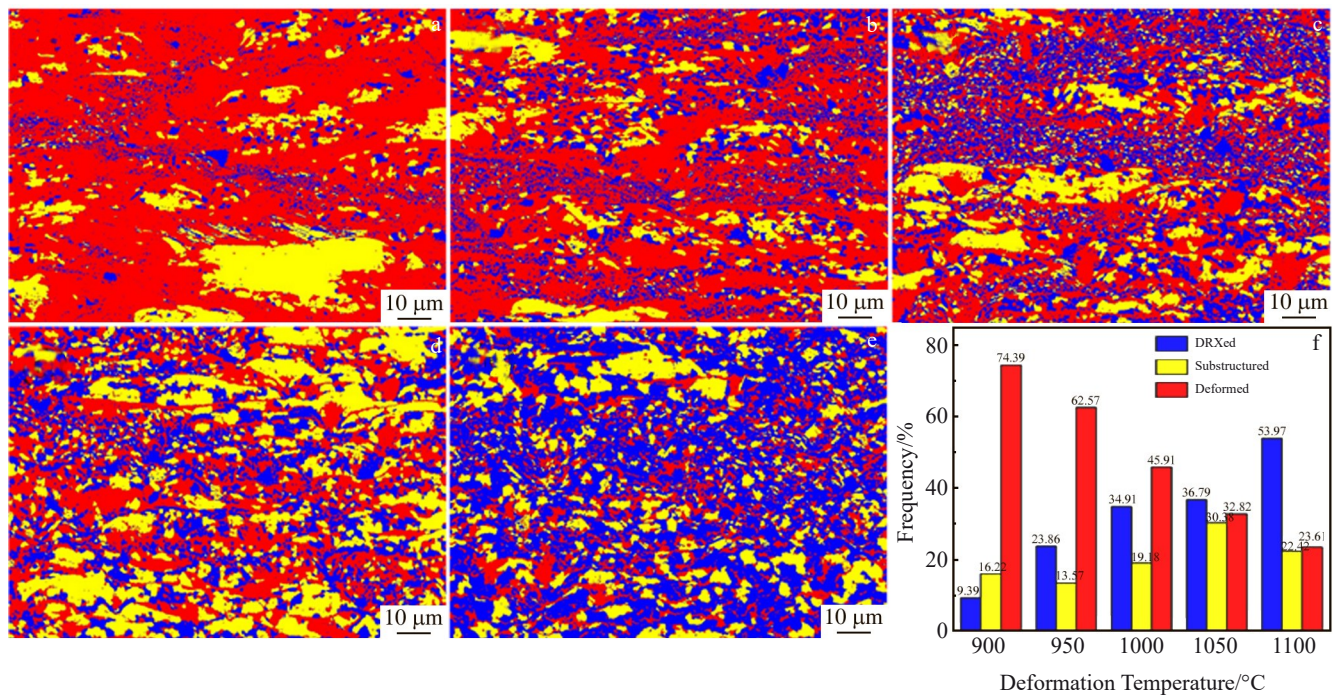


Fig.9 EBSD maps (a–e) and analysis results (f) of NiCoFeCrAl high entropy alloy after hot compression at strain rate of 0.1 s⁻¹ and temperature of 900 °C (a), 950 °C (b), 1000 °C (c), 1050 °C (d), and 1100 °C (e)

fragmented into smaller grains with more uniform distribution. The fine recrystallized grains at the grain boundaries continue to grow, and they gradually form the distortion-free equiaxial crystal.

According to Fig.9f, with the thermal deformation behavior, DRX and dynamic recovery gradually occur inside the alloy, and the primitive deformed grains are transformed into the

sub-crystalline structures and DRX grains. During this process, the NiCoFeCrAl high entropy alloy is at the low-temperature state, which provides less driving force. The NiCoFeCrAl high entropy alloy is mainly composed of primitive deformed grains with only a few fine DRX grains. With increasing the deformation temperature, DRX proportion is increased and DRX grains grow. Ultimately, the distortion-

free equiaxial crystals are formed. The original deformed grains are transformed into other structures. At deformation temperature of 900–1000 °C, the primitive deformed grains are dominated. When the temperature increases to 1050–1100 °C, the driving force is larger, and the primitive deformed grains and sub-crystalline structures are transformed into recrystallized grains. Thus, DRXed grains are dominated in this case, and the softening effect becomes more obvious, therefore effectively improving the hot deformation behavior of the alloy. Hence, the high entropy alloy under these specific thermal deformation conditions shows good thermoforming performance. In conclusion, the optimal thermal processing conditions are temperature of 980–1010 °C+strain rate of 0.01–0.001 s⁻¹ and temperature of 1050–1100 °C+strain rate of 0.01–0.1 s⁻¹.

3 Conclusions

1) The predictions based on the Prasad, Gegel, and Malas instability criteria are accurate, which is suitable for the prediction of rheological instability regions of NiCoFeCrAl high entropy alloy. However, the thermal processing map obtained by Murty instability criterion cannot present the instability region.

2) The Arrhenius constitutive model of the NiCoFeCrAl high entropy alloy can be established based on the peak stress, which can more accurately predict the peak stress under different deformation conditions.

3) The optimal thermal processing conditions are temperature of 980–1010 °C+strain rate of 0.01–0.001 s⁻¹ and temperature of 1050–1100 °C+strain rate of 0.01–0.1 s⁻¹. The high temperature provides the high driving force for the generation and transformation of dynamically recrystallized grains, and the deformation mechanism in the stable deformation region is the dynamic recrystallization.

References

- 1 Varalakshmi S, Kamaraj M, Murty B S. *Materials Science and Engineering A*[J], 2010, 527: 1027
- 2 Zhang Y, Zhou Y J. *Materials Science Forum*[J], 2007, 561: 1337
- 3 Zhang C, Zhu J, Cao W S et al. *Journal of Phase Equilibria and Diffusion*[J], 2022, 43(6): 678
- 4 Zhang W R, Liaw P K, Zhang Y. *Science China Materials*[J], 2018, 61(1): 2
- 5 Miracle D, Senkov O. *Acta Materialia*[J], 2017, 122: 448
- 6 Yang Y, He Q F. *Journal of Metals*[J], 2021, 57(4): 385
- 7 Wang J P, Zhang Z, Dai H L et al. *Corrosion Science*[J], 2022, 209: 110761
- 8 Ranganathan S. *Current Science*[J], 2003, 85(10): 1404
- 9 Chen X, Qian H, Lou Y et al. *Journal of Alloys and Compounds*[J], 2022, 920: 165956
- 10 Chen T, Shun T, Yeh J et al. *Surface and Coatings Technology*[J], 2004, 188: 193
- 11 Chen Y Y, Hong U T, Shih H C et al. *Corrosion Science*[J], 2005, 47(11): 2679
- 12 Mahesh S J, Disna S, Amit V et al. *Advanced Powder Technology*[J], 2021, 32(2): 378
- 13 Wang Fa, Jiang He, Dong Jianxin. *Rare Metal Materials and Engineering*[J], 2023, 52(1): 245 (in Chinese)
- 14 Henrique R B, Michael L, Alfred K et al. *Materials & Design*[J], 2021, 197: 109266
- 15 Chao W, Truong D P, Chunbiao W et al. *Journal of Materials Processing Technology*[J], 2021, 289: 116937
- 16 Zhang Y S, Yang Z Z, Zhou G et al. *Rare Metal Materials and Engineering*[J], 2021, 50(7): 2385
- 17 Yuan H, Liu W C. *Materials Science and Engineering A*[J], 2005, 408: 281
- 18 Jia Z, Yu L D, Wei B L et al. *Rare Metal Materials and Engineering*[J], 2022, 51(2): 461
- 19 Yao J J, Zhang D, Zhang J S. *Rare Metal Materials and Engineering*[J], 2022, 51(6): 2046
- 20 Lin Y C, Wen D X, Deng J et al. *Materials & Design*[J], 2014, 59: 115
- 21 Chen G, Chen L, Zhao G et al. *Journal of Alloys and Compounds*[J], 2017, 710: 80
- 22 Doraivelu S M, Gegel H L, Gunasekera J S et al. *Int J Mech Sci*[J], 1984, 26(9–10): 527
- 23 Malas J C, Seetharaman V. *Journal of Metals*[J], 1992, 44: 8
- 24 Prasad Y V R K, Seshacharyulu T. *Materials Science and Engineering A*[J], 1998, 243: 82
- 25 Spigarelli S, Cerri E, Cavaliere P et al. *Materials Science and Engineering A*[J], 2002, 327(2): 144
- 26 Chen Q, Hu L, Li M G et al. *Journal of Materials Engineering and Performance*[J], 2021, 31(3): 2257
- 27 Prasad Y. *Journal of Materials Engineering and Performance*[J], 2003, 12: 638
- 28 Murty S V S N, Rao B N, Kashyap B P. *Journal of Materials Processing Technology*[J], 2005, 166(2): 268
- 29 Spigarelli S, Cerri E, Cavaliere P et al. *Materials Science and Engineering A* [J], 2002, 327(2): 144
- 30 Ali S, Reza M T, Marieh A. *Materials Chemistry and Physics*[J], 2023, 295: 127213
- 31 Li Changmin, Liang Huang, Zhao Mingjie et al. *Materials Science and Engineering A*[J], 2020, 797: 139925

NiCoFeCrAl系高熵合金热加工图不同失稳判据比较

张允胜^{1,2}, 蒋学禹^{1,2}, 周 舸^{1,2}, 张浩宇^{1,2}, 张思倩^{1,2}, 车 欣^{1,2}, 陈立佳^{1,2}, 曹 雪³

(1. 沈阳工业大学 材料科学与工程学院, 辽宁 沈阳 110870)

(2. 沈阳工业大学 沈阳市先进结构材料与应用重点实验室, 辽宁 沈阳 110870)

(3. 中国航发北京航空材料研究院, 北京 100095)

摘 要: 采用Gleeble-3800热模拟试验机对NiCoFeCrAl系高熵合金进行单道次热压缩实验研究, 根据峰值应力构建了NiCoFeCrAl系高熵合金Arrhenius本构关系模型, 运用Prasad、Murty、Gegel和Malas四种失稳准则, 构建了不同失稳判据下的DMM热加工图, 并对不同失稳判据在该合金热变形过程中的适用范围进行了分析与比较, 确定了该合金的最佳热加工区间为温度为980~1010 °C+应变速率为0.01~0.001 s⁻¹和温度范围为1050~1100 °C+应变速率为0.01~0.1 s⁻¹, 平均功率耗散率大于36%。借助EBSD显微组织分析, 确定了热变形的软化机制随变形量的增大由动态回复向动态再结晶转变。

关键词: 高熵合金; 失稳判据; 热变形行为; Arrhenius本构方程; 变形组织

作者简介: 张允胜, 男, 1998年生, 硕士, 沈阳工业大学材料科学与工程学院, 辽宁 沈阳 110870, E-mail: zys086415@163.com